npj | climate and atmospheric science

Article

Published in partnership with CECCR at King Abdulaziz University

https://doi.org/10.1038/s41612-024-00605-5

Differing roles of North Atlantic oceanic and atmospheric transports in the winter Eurasian Arctic sea-ice interannual-to-decadal variability

Jiaqi Shi [1], Binhe Luo [2], Dehai Luo [1] ✉, Yao Yao [1], Tingting Gong[3,4] & Yimin Liu [5,6]

In recent decades, winter Arctic sea-ice concentration (SIC) has experienced a most prominent decline over Barents-Kara Seas (BKS). However, what regulates the time scale and spatial structure of the SIC variability over the Eurasian Arctic is unclear. Here, we find that the SIC variability over the Eurasian Arctic exhibits two major modes: decadal dipole mode with antiphase variation between the BKS and East Greenland (EG), and interannual monopole mode with in-phase variation between the BKS and EG. This decadal mode mainly results from interdecadal changes in ocean heat transports (OHTs) through Barents Sea Opening (BSO) and EG, lagging the Atlantic Multidecadal Oscillation by 7–16 years. The positive SIC dipole mode with a decrease over the BKS and an increase over the EG is also tied to the negative Arctic Oscillation comprised of Ural blocking and the negative North Atlantic Oscillation (NAO). However, the SIC loss of the interannual monopole mode mainly stems from the positive Arctic dipole comprised of Ural blocking and positive NAO through interannual changes in the BSO OHT and atmospheric moisture or heat transport. We further highlight that interannual atmospheric transports and BSO OHT associated with the Arctic dipole contribute to ~66% and ~34% of the interannual variability of the Eurasian Arctic SIC during 1960-2017, respectively. On decadal timescales, the relative contributions of atmospheric transports associated with Arctic Oscillation and OHT to the Eurasian Arctic SIC variability are ~19% and ~81%, respectively. Especially, the contribution of decadal atmospheric transports is significantly intensified during 2000–2017.

In recent decades, the winter sea-ice concentration (SIC) over the Arctic especially over the Barents-Kara Seas (BKS) has undergone an accelerated decline since the 1990s[1–3]. Rapid Arctic SIC decline in winter was found to be crucial for Arctic amplification represented by a rapid surface air temperature (SAT) rise over the Arctic region[4,5], which influences weather extremes and climate in midlatitude continents[6–12]. The BKS SIC exhibits a prominent variability on long-term trend[2,13–15], decadal[16,17] and interannual[18,19] timescales. To some extent, the abrupt decline of the winter Arctic SIC is the combined consequence of the long-term declining trend and interannual-to-decadal variability of the Arctic SIC modulated by oceanic and atmospheric processes[20], although increasing carbon dioxide (CO_2) dominates the long-term declining trend of the Arctic SIC[5,21]. Thus, further exploring the physical cause of the interannual-decadal variability of the winter BKS SIC can help us improve the understanding of the mechanism of enhanced winter Arctic warming that influences the occurrence of cold extremes over the Eurasian mid-high latitudes[6,7] and the predictability of the Arctic SIC variability[22–24].

In addition to the impact of increasing CO_2[18], the winter BKS SIC was found to be modulated by the Atlantic Multidecadal Oscillation (AMO)[18–20], Pacific Decadal Oscillation (PDO)[25,26] and El Niño-Southern Oscillation

[1]Key Laboratory of Regional Climate-Environment for Temperate East Asia, Institute of Atmospheric Physics, Chinese Academy of Sciences and University of Chinese Academy of Sciences, Beijing 100029, China. [2]State Key Laboratory of Earth Surface Processes and Resource Ecology, Beijing Normal University, Beijing 100875, China. [3]CAS Key Laboratory of Ocean Circulation and Waves, Institute of Oceanology, Chinese Academy of Sciences, Qingdao 266071, China. [4]Pilot National Laboratory for Marine Science and Technology, Qingdao 266237, China. [5]LASG, Institute of Atmospheric Physics, Chinese Academy of Science, Beijing 100029, China. [6]University of Chinese Academy of Sciences, Beijing, China. ✉e-mail: ldh@mail.iap.ac.cn

(ENSO)[19]. However, the impact of PDO on the Arctic SIC is mainly concentrated in the Pacific side[25,27], whereas the effect of AMO on the Arctic SIC is mainly located in the North Atlantic and Eurasian sides[16,17]. The AMO associated with Atlantic meridional overturning circulation (AMOC) can lead to the retreat of the Arctic SIC over the BKS via enhanced ocean heat transports (OHTs)[28,29]. The enhanced OHT can also drive the Arctic SAT variability by increasing ocean heat content in the BKS[30] because it leads the SAT variability by about 1 year[31]. The atmospheric processes have been shown to play an important role in the BKS SIC interannual variability[32]. Previous studies have revealed that the Arctic SIC shows a notable interannual variability with a high extent west of Greenland and a low extent east of Greenland, which is linked to the positive polarity of the North Atlantic Oscillation (NAO)[33,34]. When the winter Ural blocking occurs together with the positive NAO, the combined atmospheric circulation pattern is an optimal atmospheric factor that is conducive to the BKS SIC loss on intra-seasonal-to-interannual timescales due to enhanced downward infrared radiation (IR) over BKS[35,36] through increased water vapor. Some studies have indicated that the interdecadal (interannual) variability of the BKS SIC mainly comes from the Atlantic (Pacific) basin via oceanic (atmospheric) processes[17,19,30]. However, it is not clear what is the optimal mode of the decadal variability of the Eurasian Arctic SIC and whether it possesses the same mechanism as the interannual variability of the Eurasian Arctic SIC. In particular, it is not known what are the relative contributions of oceanic and atmospheric transports to the Eurasian Arctic SIC variability on decadal and interannual timescales, even though the modulation of the AMO can induce the multidecadal variability of atmospheric circulation patterns such as the NAO-like pattern[37].

In this present study, we use the reanalysis data to examine how the AMO and atmospheric circulation patterns coupled with the North Atlantic tripole influence the SIC variability over the Eurasian Arctic via changes in poleward ocean heat transports, atmospheric heat and moisture transports (see Methods). We also aim to identify what factors produce the decadal (interannual) variability of the Eurasian Arctic SIC and further estimate what are the relative contributions of oceanic and atmospheric transports to the SIC variability over the Eurasian Arctic.

Results

Interannual-decadal variability of winter sea-ice concentration (SIC) over the Eurasian Arctic

We first perform the empirical orthogonal function (EOF) analysis of winter (December-January-February, DJF) mean sea-ice concentration (SIC) anomaly in the Eurasian Arctic region (40°W-100°E, 60°-85°N) during 1950–2021 to extract the first and second EOF (EOF1 and EOF2) modes of the winter Arctic SIC anomaly and their corresponding principal

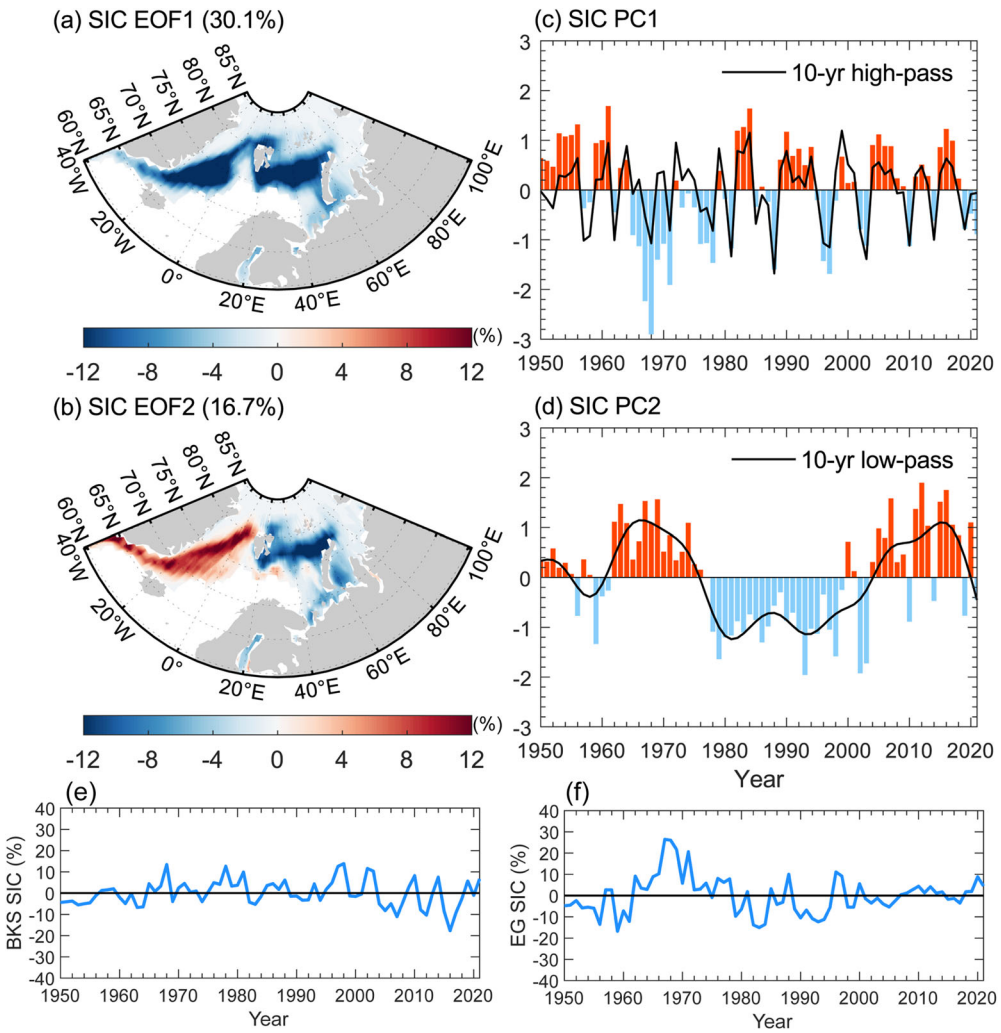

Fig. 1 | Spatial pattern and temporal variability of the winter Eurasian Arctic sea-ice concentration (SIC) during 1950-2021. a–d Spatial patterns of (**a**) first and (**b**) second empirical orthogonal function (EOF1 and EOF2) modes of the winter (December to February, DJF) mean detrended SIC (unit: %) anomaly over the Eurasian Arctic region (40°W-100°E, 60°-85°N) and (**c**, **d**) time series of their (**c**) first and (**d**) second principal components (PC1 and PC2, bars) during 1950-2021. **e**, **f** Time series of DJF-mean detrended SIC (unit: %) anomalies averaged over the (**e**) Barents-Kara Seas (30°-80°E, 65°-80°N; BKS) and (**f**) East Greenland (20°W-8°E, 70°-80°N; EG). In panel (**c**, **d**), the black line represents a 10-years (10-year) high (low) pass curve.

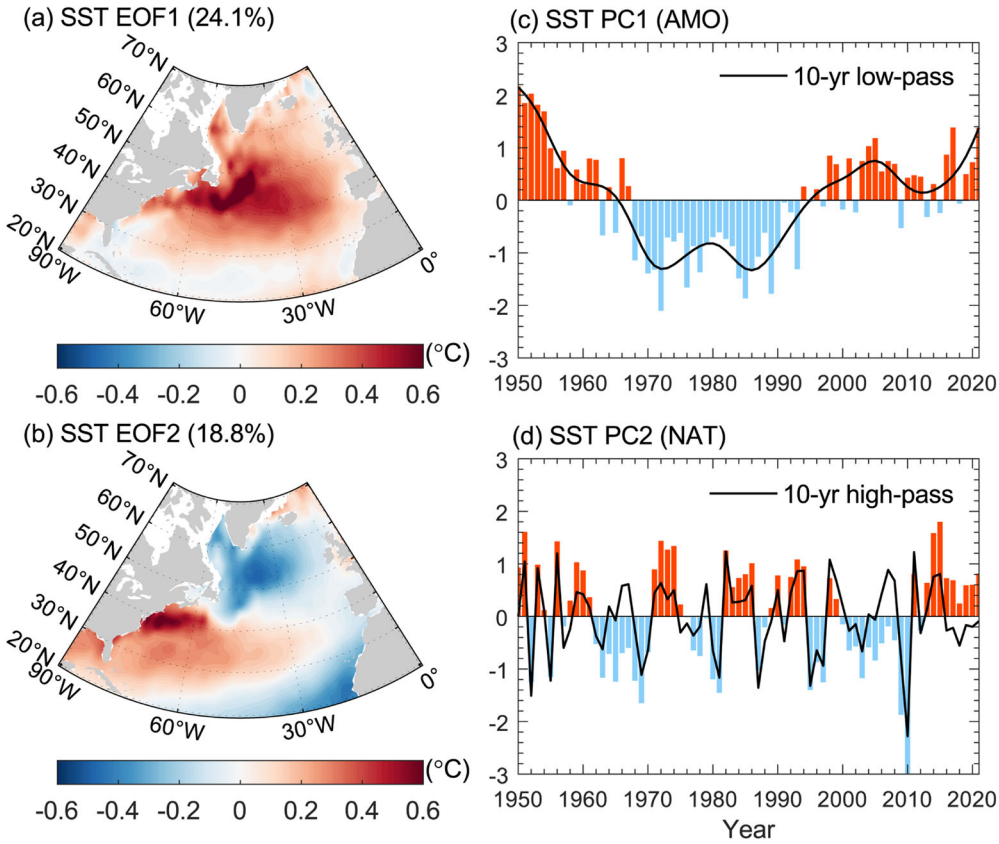

Fig. 2 | Spatial pattern and temporal variability of the winter North Atlantic SST during 1950-2021. a, **b** Spatial patterns of (**a**) first and (**b**) second empirical orthogonal function (EOF1 and EOF2) modes of the winter (December to February, DJF) mean detrended SST (unit: °C) anomaly over the North Atlantic region (90°W-0°, 20°-70°N) during 1950-2021 and (**c**, **d**) normalized time series of their (**c**) first and (**d**) second principal components (PC1 and PC2, bars) during 1950-2021. The black line represents a 10-year low pass curve in panel (**c**) as a DJF-mean Atlantic Multidecadal Oscillation (AMO) index on decadal timescales, whereas the black line represents a 10-year high-pass curve in panel (**d**) as a North Atlantic tripole (NAT) SST index on interannual timescales.

components (PC1 and PC2) (see Methods and Fig. 1). Our results show that the winter SIC EOF1 mode (Fig. 1a), which explains the 30.1% variance of the Eurasian Arctic SIC, exhibits a decrease (increase) in the Eurasian Arctic region from the East Greenland (EG, 20°W-8°E, 70°-80°N) to BKS (30°-80°E, 65°-80°N) for the positive (negative) value of the SIC PC1 time series (Fig. 1c). This mode mainly reflects the interannual variability of the Eurasian Arctic SIC (Fig. 1a, c). Because the SIC EOF1 mode shows an in-phase variation between the BKS and EG, it may be referred to as the SIC monopole mode over the Eurasian Arctic. The SIC EOF2 mode, which explains the 16.7% variance of the Eurasian Arctic SIC (Fig. 1b), exhibits a notable interdecadal variability (Fig. 1d). The east-west seesaw of the SIC anomaly between the EG and BKS is the main characteristic of this interdecadal mode, which may be referred to as the SIC dipole mode over the Eurasian Arctic. It can be defined as a positive SIC dipole with an increase in the EG and a decrease in the BKS when the SIC PC2 time series is positive. Here, we define the temporal variation with ≥10 years as the decadal variability. We further use a 10-year high (low) pass time series to characterize the interannual (decadal) variations of the Eurasian Arctic SIC, atmospheric and oceanic variables.

Our results show that the Eurasian Arctic SIC anomaly shows an amplifying variability over the BKS followed by a significant declining over the BKS after 2000 (Fig. 1e), but a decaying variability over the EG (Fig. 1f). The increased SIC variability over the BKS since the 1990s may be tied to increasing ENSO amplitude under the CO_2-induced warming climate[19] and increased OHT across the Barents Sea opening (BSO)[30,37]. While the decadal variability of the BKS SIC is mainly related to changes in OHT across the BSO[30,37–39], the physical cause of the EG SIC variability is complex. This is because the EG SIC variability does not only depend on atmospheric and oceanic heat transports on decadal timescales[28], but also on the wind-driven sea-ice drift associated with atmospheric circulation patterns[40]. However, the effect of the wind-driven sea-ice drift on the BKS SIC variability is unimportant[41]. Thus, we cannot simply use the decadal variability of atmospheric circulation patterns to explain the decadal variability of the Eurasian Arctic SIC dipole mode.

Our results further show that the interannual variability of the SIC monopole mode over the Eurasian Arctic, denoted by the SIC EOF1 (Fig. 1a), is linked to the phase of the North Atlantic tripole (NAT), represented by the SST EOF2 (Fig. 2b). They have the same main period domain (4–8 years) as seen from their wavelet power spectra (Supplementary Fig. 1a, c). For the positive value of the 10-year high pass SST PC2, the North Atlantic SST anomaly possesses a cold-warm-cold tripole structure over the North Atlantic south of Greenland (Fig. 2b), which represents the positive phase of the NAT. Previous studies have shown that the NAT is strongly coupled with the NAO[42], and the ENSO-like SST can influence NAO[43]. As a result, the interannual variability of NAT may remotely result from ENSO[19]. The ocean heat transport has been shown to be the direct cause for the interannual variation of the Eurasian Arctic SIC[44], which depends on the phase of NAT. Thus, we infer that the interannual variability of the Eurasian Arctic SIC monopole mode is in part due to the interannual modulation of the NAT, whereas the decadal variability of the SIC dipole mode over the Eurasian Arctic is linked to the interdecadal variability of the North Atlantic SST anomaly as seen from the PC1 time series of the SST EOF1 (Fig. 2a, c). This interdecadal SST EOF1 with a basin warming (Fig. 2c) mainly reflects the Atlantic multidecadal Oscillation (AMO)[45] (Supplementary Fig. 1b, d) which has a significant positive correlation ($p < 0.05$) with the SIC dipole mode denoted by the 10-year low pass SIC PC2 time series

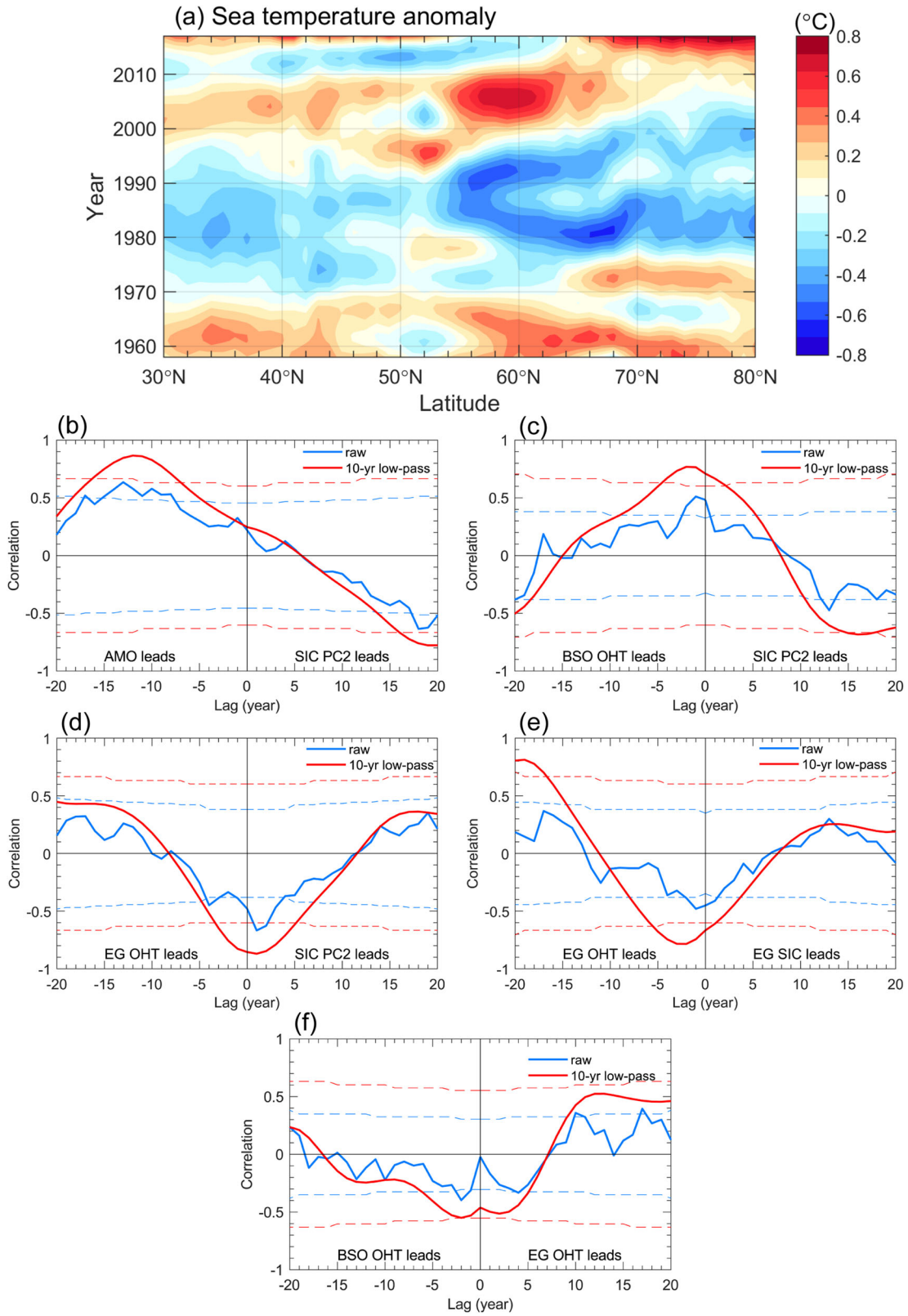

Fig. 3 | Latitude-time evolution of sea temperature anomaly and lead-lag correlation coefficients among the Eurasian Arctic sea-ice concentration (SIC) variability, oceanic heat transport (OHT) and Atlantic Multidecadal Oscillation (AMO) in winter. a Latitude-time evolution of detrended DJF-mean 10-year low pass filtered sea temperature anomaly (unit: °C) averaged from the surface to depth 300 m and over 60° W-30° E during 1958–2017. (**b**-**f**) Lead-lag correlation coefficients of the SIC PC2 with the (**b**) AMO, (**c**) BSO OHT (20°E, 71°-73°N) and (**d**) EG OHT (20°-10°W, 75°N), as well as lead-lag correlations of (**e**) EG OHT with EG SIC over the region (20°W-8°E, 70°-80°N) and (**f**) BSO OHT with the EG OHT during 1958–2017. The blue (red) curve represents the raw (10-year low pass) DJF-mean time series, whereas the blue (red) dashed lines denote the threshold being statistically significant at the 95% confidence level using the effective numbers of degrees of freedom.

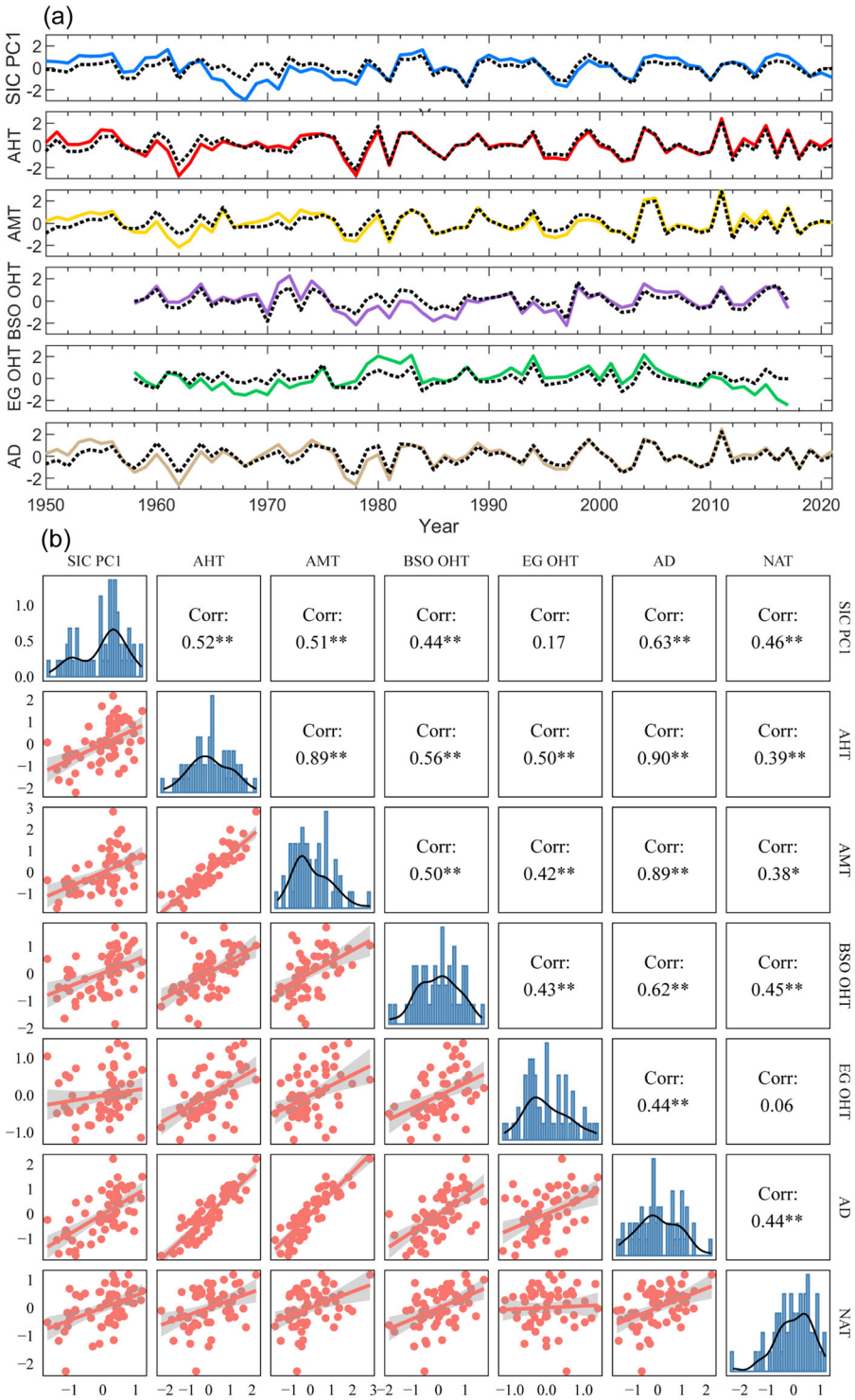

Fig. 4 | Temporal variations of the first principal component (PC1) time series of the winter (DJF-mean) Eurasian Arctic sea-ice concentration (SIC) anomaly and atmospheric transports during 1950-2021 and ocean heat transports during 1958-2017. a Normalized time series of the first principal component (PC1) of the winter (DJF-mean) SIC anomaly over the Eurasian Arctic (40°W-100°E, 60°-85°N), the Arctic dipole (AD) index as defined by the PC2 time series of the winter Z500 anomaly north of 70°N (Supplementary Fig. 2), meridional atmospheric heat transport (AHT) and atmospheric moisture transport (AMT) anomalies over the Arctic region (20°W-80°E, 70°-80°N) during 1950-2021 and the winter ocean heat transports (OHTs) through the Barents Sea opening (BSO) (20°E, 71°-73°N) and East Greenland (EG) (20-10°W, 75°N) during 1958-2017. **b** Probability density functions (bars) of the 10-year high pass (dashed lines in Fig. 4a) SIC PC1, AHT, AMT, BSO OHT, EG OHT, AD and NAT indices and their correlation coefficients during 1958–2017, where the NAT index is defined in Fig. 2d. The one (two) asterisk represents the correlation being statistically significant at the 95% (99%) confidence level. The black line denotes a fitting curve, whereas the red line represents the slope rate of the scatter diagram between each two indices.

(Fig. 1d), when it leads the SIC dipole mode by 7–16 years (Fig. 3b). In fact, when the AMO is in a positive phase (Fig. 2a), the Atlantic warm water as denoted by the warm SST anomaly can intrude into the high latitude Arctic (e.g., BKS) along the east side of the North Atlantic since the 2000s (Fig. 3a) to cause the melting of the BKS SIC due to increased oceanic heat contents[46]. However, as we note below, the southward shift of the cold water from the high-latitude Arctic to the EG during the positive AMO phase period is also an important factor leading to an increase in the SIC anomaly over the EG. Thus, the decadal variability of the SIC dipole mode over the Eurasian Arctic is likely induced by the AMO. However, previous studies did not quantify the contributions of oceanic and atmospheric transports to the two modes of the Eurasian Arctic SIC variability on interannual and decadal timescales.

Potential drivers of the winter Eurasian Arctic SIC interannual-decadal variability

We first discuss what drives the interannual variability of the Eurasian Arctic SIC monopole mode, even though the interannual variability of SIC is partly

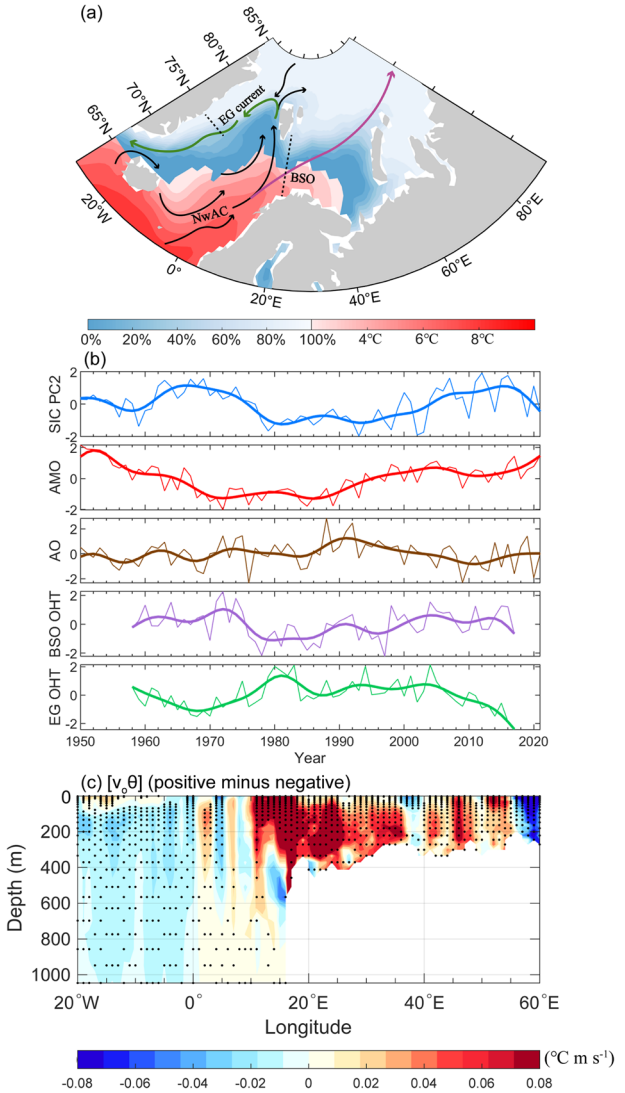

Fig. 5 | Schematic diagram of ocean currents over North Atlantic and Eurasian Arctic, the temporal variations of winter Eurasian Arctic sea-ice concentration (SIC), atmospheric circulation pattern and ocean heat transports and the decadal variation of the meridional oceanic heat transport. a Schematic plot of the Eurasian Arctic with ocean currents over the North Atlantic. The black arrows denote the main ocean currents over the North Atlantic (Norwegian warm Atlantic Current is referred to as NwAC), the ocean current in the north boundary of Oddens over the Eastern Greenland (EG) from the high latitude Arctic is referred to as the EG current (green arrows). The black dot lines represent the sections of the Barents Sea Opening (BSO, 20°E, 71°-73°N) and EG (20°-10°W, 75°N). **b** Normalized time series of the second principal component (PC2) of the winter (DJF-mean) SIC anomaly over the Eurasian Arctic (40°W-100°E, 60°-85°N), the Arctic oscillation (AO) index as defined by the PC1 time series of the winter Z500 anomaly north of 70°N (Supplementary Fig. 2a), Atlantic Multidecadal Oscillation (AMO) index, and the ocean heat transports (OHTs) through BSO and EG on decadal timescales as denoted by 10-year low pass curves (thick lines). **c** Longitude-depth profile of the difference of the meridional oceanic heat transport $[v_o\theta]$ (unit: °C m s^{-1}) averaged over 65°-80°N between the positive (≥0.5 STDs) and negative (≤−0.5 STDs) phases of the normalized SIC PC2 time series, where the square bracket represents a meridional average and v_o (θ) denotes the 10-year low-pass filtered oceanic meridional velocity (sea temperature). Dots represent the region being statistically significant at the 95% confidence level.

linked to NAT as noted above. Our calculation further shows that the 10-year high pass SIC PC1 time series has a high simultaneous positive correlation of 0.46 ($p < 0.01$) with NAT (Fig. 4b and Supplementary Fig. 3b). Because the NAT is coupled with the interannual AMOC and NAO-like pattern on interannual timescales[45], the interannual variability of the Eurasian Arctic SIC monopole mode is inevitably linked to changes in the OHT, atmospheric heat and moisture transports (AHT and AMT) on interannual timescales[36]. In this study, we focus on the roles of meridional AHT and AMT because the zonal component of the moisture or heat transport is insignificant for the SIC variability over BKS[47]. In fact, the AHT mainly influences the SIC via the air temperature change, whereas the AMT mainly changes the SIC through the variation of the downward IR due to the water vapor change. Here, we calculate the meridional AHT and AMT anomalies integrated over the Arctic region (20°W-80°E, 70°-80°N) as the AHT and AMT entering the Eurasian Arctic (see Methods). We find that the AHT and AMT show dominant interannual variations (dashed lines in Fig. 4a) and a high simultaneous positive correlation of 0.89 ($p < 0.01$) (Fig. 4b). Our results show that the 10-year high pass SIC PC1 time series has a simultaneous positive correlation of 0.52 or 0.51 ($p < 0.01$) (Fig. 4b) with the 10-year high pass AHT or AMT index (dashed line in Fig. 4a). This indicates that the interannual variability of the Eurasian Arctic SIC monopole mode comes partly from interannual changes in AHT and AMT[35,36]. Moreover, the 10-year high pass AHT (AMT) index has a simultaneous positive correlation of 0.90 (0.89) ($p < 0.01$) (Fig. 4b) with the 10-year high pass Arctic dipole index (dashed line in Fig. 4a) as defined by the PC2 time series of the second EOF mode of the winter 500-hPa geopotential height (Z500) anomaly north of 70°N (Supplementary Fig. 2b, e)[48]. Thus, the interannual variability of the AHT or AMT is mainly dominated by the interannual Arctic dipole. This is because the positive Arctic dipole (i.e., the positive value of the DJF-mean Z500 PC2 time series in Supplementary Fig. 2d) shows a notable interannual variability and consists of Ural blocking and the positive NAO (NAO$^+$) pattern (Supplementary Fig. 2e). When Ural blocking occurs together with the NAO$^+$-like pattern, warm moisture over the North Atlantic can be transported to the Eurasian Arctic via the relay effect of the Ural blocking and NAO$^+$ patterns to result in a significant increase in water vapor over the Eurasian Arctic[36]. As a result, the positive Arctic dipole favors intensified surface air warming over the Eurasian Arctic to induce enhanced melting of the Eurasian Arctic SIC due to intensified downward infrared radiation (IR) associated with increased water vapor over the Eurasian Arctic from the EG to BKS[36,49]. Thus, the interannual Eurasian Arctic SIC monopole mode has a significant positive simultaneous correlation of 0.63 ($p < 0.01$) with the Arctic dipole (AD) index (Fig. 4b and Supplementary Fig. 3a), even though the winter Arctic dipole is coupled with the NAT via the NAO component (the simultaneous correlation coefficient between the Arctic dipole and NAT is 0.44 ($p < 0.01$) (Fig. 4b)). This implies that the presence of a positive Arctic dipole can lead to the interannual decline of the Eurasian Arctic SIC via enhanced AHT or AMT. Thus, the phase of the Arctic dipole can significantly influence the interannual variability of the Eurasian Arctic SIC monopole mode partly through the interannual changes in the AHT or AMT. As noted below, the interannual change in the BSO OHT can also affect the interannual variability of the BKS SIC.

Here, we calculate the zonal OHT anomaly integrated over the BSO region (20°E, 71°-73°N) as the BSO OHT, whereas the meridional OHT anomaly integrated over the north boundary region (20°-10°W, 75°N) of Oddens is calculated as the EG OHT (Methods and Fig. 5a). Our results reveal that the interannual variability of the Eurasian Arctic SIC is linked to the interannual variation of the poleward intrusion of North Atlantic warm water as denoted by the BSO OHT because the SIC PC1 has a significant simultaneous positive correlation of 0.44 ($p < 0.01$) with BSO OHT during 1958-2017 for the 10-year high pass time series (Fig. 4a–b). But they have no significant correlation on decadal timescales as denoted by a 10-year low pass filtered curve (Fig. 6a). When the Arctic dipole is in a positive phase, the wind-driven interannual warm water by the NAO$^+$ component of the positive Arctic dipole can in part intrude into the Eurasian Arctic across the BSO and Norwegian Sea (Fig. 6b)[30,37] via interannual variations in the AMOC associated with ENSO[50]. This process favors increased BSO OHT to result in the decline of the BKS SIC due to the emergence of warm water over the

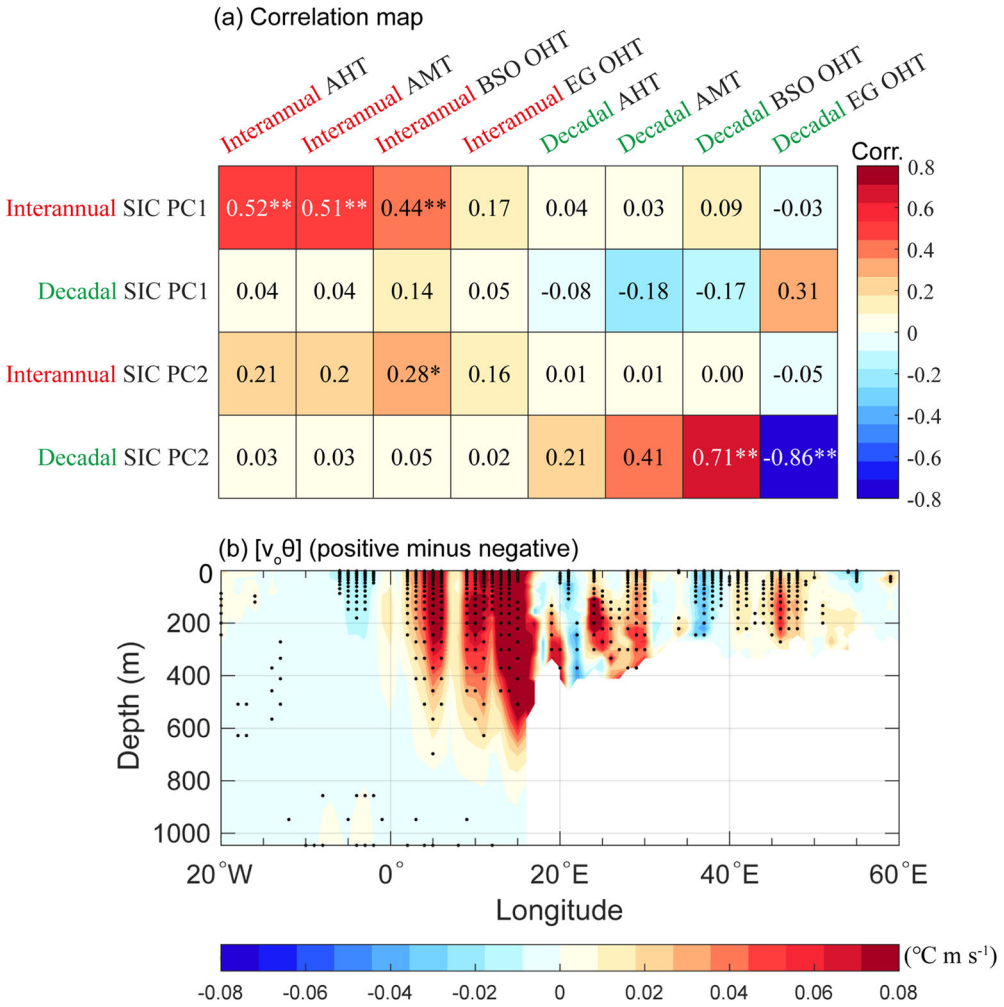

Fig. 6 | Correlation map among the principal components (PC1 and PC2) time series of winter Eurasian Arctic sea-ice concentration (SIC), atmospheric transports and ocean heat transports on interannual-decadal scales, and the interannual variation of meridional oceanic heat transport in winter. **a** Correlation coefficients of the normalized DJF-mean SIC PCs with the atmospheric and oceanic transports during 1958–2017. The correlation coefficient being statistically significant at the 95% (99%) confidence level is indicated by one (two) asterisk. **b** Longitude-depth profile of the difference of the meridional oceanic heat transport [$v_o\theta$] (unit: °C m s^{-1}) averaged over 65°-80°N between the positive (≥0.5 STDs) and negative (≤−0.5 STDs) phases of the normalized SIC PC1 time series, where the square bracket represents a meridional average and v_o (θ) denotes the 10-year high pass filtered oceanic meridional velocity (sea temperature). The 95% confidence level region is marked by dots.

Eurasian Arctic. To some extent, the Arctic dipole can significantly influence the interannual variability of the BKS SIC via the interannual variation of the BSO OHT because the AD index has a significant simultaneous positive correlation of 0.62 ($p < 0.01$) with the 10-year high pass BSO OHT time series (Fig. 4b, Supplementary Fig. 3c).

While the EG OHT has a significant simultaneous positive correlation of 0.44 ($p < 0.01$) with the AD index (Fig. 4b, Supplementary Fig. 3d), increased interannual EG OHT does not significantly contribute to the interannual melting of the Eurasian Arctic SIC in the east of Greenland in that the EG OHT and SIC PC1 have only a weak simultaneous positive correlation of 0.17 ($p > 0.1$) for 10-year high pass time series (Fig. 4b). It seems that the increased AHT or AMT on interannual timescales mainly contributes to the interannual SIC loss over the Eurasian Arctic, even though the increased BSO OHT mainly causes the interannual SIC decline in the eastern part (i.e., BKS) of the Eurasian Arctic. Thus, we present a finding that the interannual BSO OHT mainly influences the SIC over BKS (i.e., the east part of Eurasian Arctic), whereas the interannual AHT or AMT primarily affects the overall Eurasian Arctic SIC from EG to BKS. This indicates that the AHT or AMT and BSO OHT on interannual timescales play different roles in the interannual variability of the Eurasian Arctic SIC monopole mode. This result was not noted in previous studies[46], although there is an anticorrelation between the Atlantic OHT north of 60°N and the Arctic SIC on interannual timescales[28]. Consequently, increased interannual BSO OHT and AHT or AMT due to the presence of a positive Arctic dipole coupled with the interannual NAT having a cold-warm-cold SST tripole are key factors leading to a decrease in the interannual SIC over the Eurasian Arctic. This result suggests that the Arctic dipole (Fig. 7a, Supplementary Fig. 2e) is an optimal atmospheric circulation that leads to the interannual variability of the SIC monopole mode over the Eurasian Arctic (Fig. 7c).

Here, we further account for what causes the decadal variability of the SIC dipole mode over the Eurasian Arctic as represented by the 10-year low pass SIC PC2 time series (Fig. 1d). We can see that the positive SIC dipole with an increase in EG and a decrease in BKS mostly occurs during 2000-2021, but an opposite SIC dipole appears during 1970-1999 (Fig. 1e, f). Such a decadal variability is tied to the interdecadal alternation of warm and cold sea temperature anomalies over the North Atlantic basin (Fig. 3a) associated with the phase shift of the AMO (Fig. 2a, c). It is further found that the pronounced poleward migration of the warm SST anomaly north of 50°N seems to happen mainly after 2000 (Fig. 3a), which is also accompanied by increased meridional ocean heat transports induced by the Norwegian warm Atlantic Current (NwAC, the northernmost extension of the Gulf Stream) in the

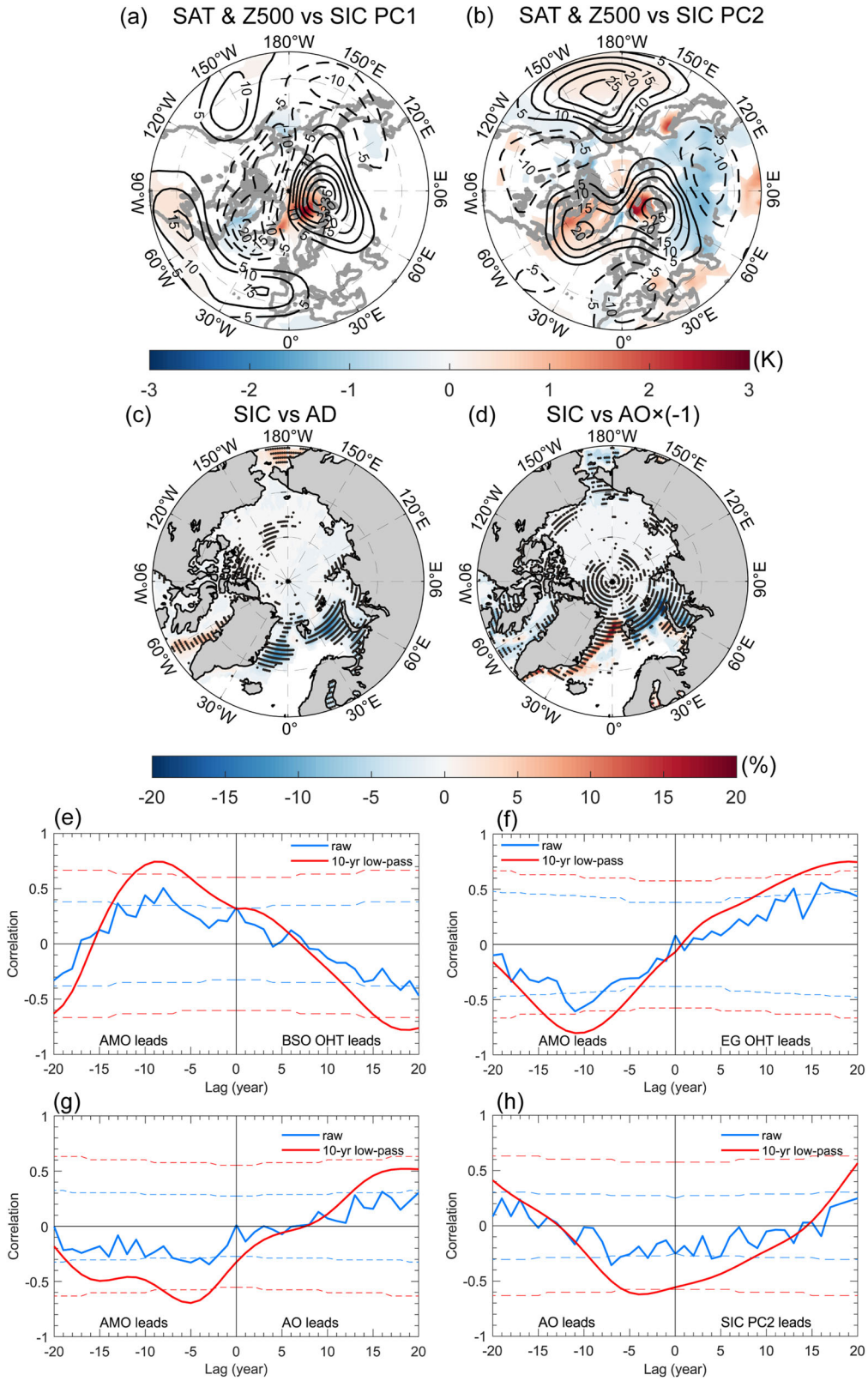

upper North Atlantic and the cold current from high latitude Arctic region to the EG (Fig. 5a). Our results suggest that the phase alternation of the AMO may lead to the decadal variability of the SIC dipole between BKS and EG probably via interdecadal out-phase changes in BSO OHT and EG OHT (Fig. 5b). In fact, the SIC PC2 also has a significant simultaneous correlation with the BSO OHT or EG OHT even for 10-year low pass time series (Fig. 3c, d). Such a causal relationship can be further explained by calculating the lead-lag correlations of the 10-year low pass AMO index with the 10-year low pass BSO OHT and EG OHT indices. It is noted that the AMO index has a significant positive correlation ($p < 0.05$) with the 10-year low pass SIC PC2 time series when the AMO leads the SIC dipole mode by about 7–16 years (Fig. 3b), which is consistent with the ocean advection speed of about 5 cm s^{-1}

Fig. 7 | Winter atmospheric circulation patterns related to the interannual-decadal variability of the Eurasian Arctic sea-ice concentration (SIC) anomaly and relationships among Atlantic Multidecadal Oscillation (AMO), Arctic Oscillation (AO), the Eurasian Arctic SIC dipole mode and ocean heat transports. a, **b** Regressed DJF-mean Z500 (contours, unit: gpm) and SAT (color shading, unit: K) anomalies against the normalized time series of (**a**) 10-year high pass filtered first principal component (PC1) and (**b**) 10-year low pass filtered second principal component (PC2) of the Eurasian Arctic SIC anomaly. **c**, **d** Regressed DJF-mean SIC (color shading, unit: %) anomalies against the normalized time series of (**c**) interannual Arctic dipole (AD) as denoted by the 10-year high pass PC2 time series of the winter Z500 anomaly north of 70°N and (**d**) decadal negative Arctic oscillation (AO) index as denoted by the 10-year low pass PC1 time series of the winter Z500 anomaly north of 70°N multiplied by −1. **e**–**h** Lead-lag correlation between normalized DJF-mean AMO, AO, SIC PC2 and ocean heat transports (OHTs) across BSO and EG with raw (blue line) and 10-year low pass (red line) curves. The blue (red) dashed line denotes the threshold being statistically significant at the 95% level for unsmoothed (smoothed) time series using the effective numbers of degrees of freedom, whereas the 95% confidence level region in panels (**a**, **b**, **c**, **d**) is marked by the color shading (dots).

from North Atlantic to the Arctic[37]. In particular, they have a largest positive correlation of 0.87 ($p < 0.05$) when the AMO leads the SIC dipole by ~11 years (Fig. 3b). This suggests that the decadal SIC dipole mode with an increase over the EG and a decrease over the BKS is attributed to the positive phase of AMO through increased BSO OHT and reduced EG OHT (or increased negative EG OHT from the high latitude Arctic) because the BSO (EG) OHT has significant positive (negative) correlations ($p < 0.05$) with the AMO when the AMO leads the BSO (EG) OHT by 5–11 (7–14) years (Fig. 7e, f). In particular, the BSO (EG) OHT has a largest positive (negative) correlation of 0.74 (−0.80) with the AMO when the AMO leads the BSO (EG) OHT by ~9 (~11) years. This means that the AMO and BSO OHT change in-phase, whereas the EG OHT and AMO change in antiphase. Thus, the positive phase of the AMO tends to favor enhanced BSO OHT and reduced EG OHT to result in the decadal variability of the SIC dipole between the BKS and EG, which is likely linked to enhanced horizontal ocean circulation in Nordic Seas[51].

Here, we further explain why the Eurasian Arctic SIC anomaly exhibits an east-west dipole structure only on decadal timescales. This aim can be reached by calculating the longitude-depth profile of the difference of the meridional oceanic heat transport [$v_o\theta$] (where v_o is the meridional oceanic velocity and θ is the sea temperature) averaged over 65°-80°N between the positive and negative phases of the 10-year low pass SIC PC2 time series. Our results show that the meridional heat transport to the Eurasian Arctic mainly appears in the upper 400 m and is enhanced in the east of 10°E, but reduced in the longitude region (20°W-0°) (Fig. 5c). This result is consistent with the opposite variation of the OHT between the BSO and EG on decadal timescales which is regulated by the AMO phase transition. However, the meridional ocean heat transport [$v_o\theta$] on interannual timescales is relatively weak and is mainly located in the west of 20°E (Fig. 6b). Thus, the dipole structure of the Eurasian Arctic SIC mainly behaves as a decadal variability. On the other hand, we see that for a 10-year low pass filtered data the BSO OHT has a largest positive (negative) correlation of 0.77 (−0.55) with the Eurasian Arctic SIC dipole mode (EG OHT) when the BSO OHT leads the SIC PC2 (EG OHT) by ~2 years (Fig. 3c, f), whereas the EG OHT has a largest negative correlation of −0.80 with the EG SIC when the EG OHT leads ~2 years (Fig. 3e). This indicates that the decadal variation of the Eurasian Arctic SIC dipole is not synchronous with that of the EG SIC and they have a small phase mismatch of ~2 years. While the positive SIC dipole over the Eurasian Arctic is comprised of a negative SIC anomaly over the BKS and a positive anomaly over the EG, the SIC anomalies in the two regions do not have a significant correlation on decadal timescales. This reflects that the decadal variations of the BKS and EG anomalies of the Eurasian Arctic SIC dipole have different oceanic contributors.

Different contributions of atmospheric and oceanic transport processes to the interannual-decadal variability of the winter Eurasian Arctic SIC

Here, we use the 10-year low pass time series of the winter Z500 PC1 to define the decadal winter Arctic Oscillation (AO) (Supplementary Fig. 2c). While the interannual loss of the Eurasian Arctic SIC, as denoted by the 10-year high pass SIC PC1 (Fig. 1c), corresponds to a positive Arctic dipole pattern consisting of Ural blocking and positive NAO (Supplementary Fig. 2b, d), its decadal positive SIC dipole, as represented by the positive value of the l0-year low pass SIC PC2 (Fig. 1d), corresponds to a negative AO-like pattern comprised of Ural blocking and negative NAO (Supplementary Fig. 2a, c). Thus, it is inferred that the decadal variability of the SIC dipole between the BKS and EG is also linked to the decadal variability of the Arctic Oscillation (Fig. 7b). The negative AO has been shown to dominate the decadal variability of the Eurasian cold anomaly[52,53], whereas the positive Arctic dipole mainly determines the interannual variability of the Eurasian cold anomaly[52]. Our results further reveal that the 10-year low pass AO index has a largest negative correlation of −0.70 ($p < 0.05$) with the 10-year low pass AMO index when the AMO leads the AO by ~5 years (Fig. 7g). The AO index does also have a maximum negative correlation of −0.62 ($p < 0.05$) with the Eurasian Arctic SIC dipole mode when the AO leads ~3 years (Fig. 7h). This suggests that the decadal variation of the AO pattern is an important atmospheric factor for the decadal variability of the SIC dipole between the BKS and EG (Fig. 7d), because the SAT of these two regions is different under the regulation of AO pattern (Supplementary Fig. 2f). In particular, the negative AO favors the negative EG OHT to result in an increase in the EG SIC because the EG OHT has a largest positive correlation of 0.65 ($p < 0.05$) with the AO index when the AO leads ~5 years (Supplementary Fig. 3f). In fact, the negative NAO or Greenland blocking component of the negative AO is also conducive to the southward shift of cold airs to the EG, which favors an increase in the EG SIC. However, the effect of the decadal AO is relatively weak compared to the impact of the EG OHT. This is because the Eurasian SIC dipole mode has a simultaneous negative correlation of -0.85 with the EG OHT, but it has a largest correlation of −0.62 with the AO when the AO leads ~3 years (Figs. 7h, 3d). For the impact of negative AO-like pattern on BKS SIC, its Ural blocking component can transport heat and moisture to the BKS to result in a decrease in the BKS SIC[35], although the AO index lags the BSO OHT by ~9 years (Supplementary Fig. 3e). The decadal BSO OHT in the upper layer ocean is main driver of the decadal variability of the BKS SIC (Fig. 3c). We further see that the 10-year low pass BSO OHT has a largest negative correlation of −0.55 ($p < 0.05$) with the 10-year low pass EG OHT when the BSO OHT leads ~2 years (Fig. 3f). Thus, the decadal AO pattern and the opposite variation of the decadal OHT between the BSO and EG (Fig. 3f) combine to produce the decadal variability of the SIC dipole between the BKS and EG.

Because the negative AO-like pattern is comprised of the negative NAO and Ural blocking patterns, it is not only coupled with the North Atlantic SST anomaly via the NAO, but also coupled with the BKS SIC anomaly via Ural blocking. Thus, the lead-lag relationships between the AO and AMO are not stationary unlike those of the AMO with the BSO OHT. Our results reveal that the AMO and BSO OHT have a stationary significant positive correlation when the AMO leads the BSO OHT by ~9 years (Supplementary Fig. 4a, b). In contrast, the AO has a non-stationary significant correlation with the AMO (Supplementary Fig. 4c, d). Instead, their significant negative correlation takes place mainly after 1997 when the AMO leads the AO by ~5 years, even though the SIC dipole mode has a significant negative correlation with the AO after 2000 under a time lag of ~3 years. Thus, we can infer that the OHT and AO can jointly strengthen the decadal variability of the Eurasian Arctic SIC dipole mainly after 2000. This may explain why the BKS SIC decline of the Eurasian Arctic SIC dipole exhibits a decadal intensification, while the EG SIC exhibits an opposite change.

Next, we use a multiple linear regression equation (Methods) to approximately evaluate the relative contributions of the atmospheric transport and ocean heat transport to the Eurasian SIC variability on interannual and decadal timescales if the variance inflation factors of the

atmospheric and oceanic variables (i.e., AHT, AMT, BSO OHT, EG OHT and AO) with the principal components (PC1 and PC2) of the Eurasian Arctic SIC are smaller than 10. It is easily estimated that during 1960–2017 the relative contributions of the atmospheric transport and OHT to the interannual Eurasian SIC variability are 66% and 34%, respectively. It can also be found that the relative contributions of the decadal atmospheric transport and OHT to the decadal Eurasian SIC variability are 19% and 81% during 1960–2017, which become 48% and 52% during 2000–2017. Clearly, the role of the atmospheric transport in the decadal Eurasian SIC variability is intensified during 2000–2017 compared to during 1960–1999[54].

Discussion

In this study, we have examined the different roles of the ocean heat transport and atmospheric heat or moisture transport in the interannual-to-decadal variability of the winter SIC over the Eurasian Arctic. Two modes of the SIC variability over the Eurasian Arctic are found, which are the interannual monopole mode with an in-phase variation between the BKS and EG and the decadal dipole mode with an antiphase variation between the BKS and EG, respectively. The interannual variability of the Eurasian Arctic SIC with a monopole structure is shown to mainly results from the atmospheric heat and moisture transports, and BSO OHT associated with the Arctic dipole on interannual timescales. The interannual loss of the Eurasian Arctic SIC is mainly related to the positive AD consisting of Ural blocking and the positive phase of NAO[36]. However, the decadal variability of the Eurasian Arctic SIC with a zonal dipole between the BKS and EG is mainly produced by the opposite decadal variation of the OHT between the BKS and EG, which is related to the phases of AMO and AO via decadal changes in the OHT and atmospheric transport. When the Eurasian Arctic SIC shows a decadal dipole mode with an increase in the EG SIC and a decrease in the BKS SIC, it is found to be linked to the positive AMO and a negative AO consisting of Ural blocking and the negative NAO on decadal timescales.

Moreover, we also found that the interannual atmospheric transport associated with the AD plays a more significant role in the interannual variability of the Eurasian Arctic SIC during 1960–2017 than the interannual BSO OHT. However, the decadal OHT associated with the AO and AMO plays a major role in the decadal variability of the Eurasian Arctic SIC dipole during 1960–2017, even though the contribution of atmospheric transports is intensified during 2000–2017.

However, it must be pointed out that the relative contributions of atmospheric transport and OHT to the winter SIC variability over the Eurasian Arctic estimated here are based on the multiple linear regression model and reanalysis data. Whether such estimates are precise deserves further investigations from the CMIP6 models and numerical modelling.

Methods

Data

The observed monthly sea-ice concentration (SIC) and sea surface temperature (SST) data are from the U.K. Met Office Hadley Centre SIC and SST (HadISST) dataset[55], with a 1° resolution for winter (December-February, DJF hereafter) covering the period from December 1950 to February 2022 (1950–2021 winter, hereafter). The oceanic data including potential sea temperature and meridional/zonal velocity are taken from Ocean Reanalysis System 5 (ORAS5) reanalysis[56], with a 1° resolution and 75 vertical levels, from December 1958 to February 2018 (1958–2017 winter, hereafter). The geopotential height, meridional/zonal wind, air temperature and specific humidity data are from National Center for Environmental Prediction/National Center for Atmospheric Research (NCEP/NCAR) Reanalysis[57], for the period from December 1950 to February 2022 (1950–2021 winter, hereafter) with a 2.5° resolution and 17 vertical pressure levels.

The definition of interannual and decadal variations

We use a fourth-order Butterworth filter[58] to separate high- and low-frequency variations (i.e., interannual versus decadal). Interannual variations are obtained by using 10-year high pass filter, whereas decadal variations are derived by using 10-year low pass filter. The testing using different filter windows with 9 years and 11 years is also made. Similar results are found (not shown).

Empirical Orthogonal Function (EOF) decomposition of anomaly fields and the index definition of Atlantic Multidecadal Oscillation and North Atlantic tripole

We apply Empirical Orthogonal Function (EOF) analysis to linearly detrended winter mean SIC anomaly over the Eurasian Arctic (40°W-100°E, 60°-85°N) and SST anomaly over the North Atlantic (90°W-0°, 20°-70°N) during the winter (DJF-mean) of 1950–2021 to obtain two leading modes and their corresponding principal component (PC) time series. Here, the 10-year high pass (low pass) filtered PC1 (PC2) timeseries of the SIC EOF1 (EOF2) mode is used to characterize the interannual (decadal) variability of the Eurasian Arctic SIC. Also, the 10-year low pass filtered PC1 timeseries of the North Atlantic SST EOF1 is used to define the Atlantic Multidecadal Oscillation (AMO) on decadal timescales, whereas the 10-year high pass filtered PC2 timeseries of the North Atlantic SST EOF2 is defined as the interannual variability of the North Atlantic SST as denoted by the North Atlantic tripole (NAT).

Wavelet spectrum analysis

We apply the wavelet spectrum analysis[59] with Morlet wavelet base to 10-year high pass PCs, and Paul wavelet base to 10-year low pass PCs in order to see whether the filtered PCs have significant periodic oscillations.

Calculating the ocean heat transport (OHT)

We calculate meridional ocean heat transport (OHT) through East Greenland (EG) at 75°N, which is given by the following equation[60]:

$$OHT_{EG}(t) = \rho C_p \int_{x1}^{x2} \int_{z}^{0} v_o \theta \, dz dx \tag{1}$$

where ρ is the density of seawater (1027 kg m^{-3}), which is assumed to be uniform; C_p is the heat capacity of seawater (3985 J kg^{-1}°C^{-1}); z is the ocean depth which sets as −300m; $x1$ and $x2$ are the longitude limits which are set as 20°W and 10°W; v_o is the monthly meridional velocity of ocean, and θ is the monthly potential temperature of seawater.

The zonal OHT through Barents Sea Opening (BSO) at 20°E is given by the following equation[60]:

$$OHT_{BSO}(t) = \rho C_p \int_{y1}^{y2} \int_{z}^{0} u_o \theta \, dz dy \tag{2}$$

y1 and y2 are the latitudes which are chosen to be 71°N and 73°N, and u_o is the monthly zonal velocity of ocean. ρ, C_p, z and θ are defined the same as Eq. (1). The winter time series of OHT_{EG} and OHT_{BSO} in Eqs. (1, 2) are computed during 1958–2017.

Calculating atmospheric heat and moisture transports (AHT and AMT)

The poleward atmospheric heat transport (AHT) at each grid is estimated by the following equation[47]:

$$AHT = -\frac{1}{g} \int_{sfc}^{top} v_a T dp \tag{3}$$

where v_a is the northward velocity, T is the air temperature, g is the gravitational acceleration; sfc denotes 1000hPa and top is chosen as 10hPa.

The poleward atmospheric moisture transport (AMT) at each grid is as follows[47]:

$$AMT = -\frac{1}{g} \int_{sfc}^{top} v_a q dp \tag{4}$$

where q is the specific humidity, and the definition of other variables are the same as Eq. (3).

The winter AHT and AMT in Eqs. (3, 4) are calculated for 1950–2021. Then we compute domain-averaged AHT and AMT anomalies over the Eurasian Arctic region (20°W-80°E, 70°N-80°N) to explore their influence on the Eurasian Arctic SIC.

Data treatment and statistical significance test

All anomaly fields are obtained by removing seasonal cycle and linear trend at each grid point. The linear trend represents the global warming. Two-sided Student's *t*-test is used in the significance testing of composite fields and the correlation between two variables, with the effective degree of freedom as defined by[61]

$$N_{\text{eff}} = \frac{N}{\max\left[1, 1 + 2\sum_{\tau=1}^{\tau_{\max}}\left(1 - \frac{\tau}{N}\right) r_X(\tau) r_Y(\tau)\right]} \quad (5)$$

Here, N denotes the time series length, and r_X (τ) and r_Y (τ) are the autocorrelations of time series X and Y at lag τ years. τ_{max} is set as the maximum lag year.

Multiple linear regression model

To explore the relative contribution of oceanic and atmospheric transports to the SIC variability, a multiple linear regression model for interannual and decadal SIC variability is derived using different predictors that significantly correlate ($p < 0.05$) with SIC PC1 and PC2 time series. Each variable is normalized to calculate the standardized regression coefficients. The fit has the form:

$$Y(t) = \sum_{k=1}^{n} \beta_k X_k(t) \quad (6)$$

Where $Y(t)$ is the normalized time series of the SIC PC1 or PC2, and $X_k(t)$ is the corresponding normalized affecting factors at t year, β_k is the standardized regression coefficient. We use standardized regression coefficients to measure the relative contribution (C_{x_k}) of different factors (X_k) to $Y(t)$ as follow[62,63]:

$$C_{x_k} = \frac{|\beta_k|}{\sum_{k=1}^{n} \beta_k} \quad (7)$$

Multiple linear regression model for the interannual variability of SIC

We use the normalized 10-year high pass filtered time series of AHT, AMT, and BSO OHT to account for the relative contributions of the atmospheric transport and OHT to the interannual variability of the SIC PC1 over the Eurasian Arctic. Calculating the regression coefficients by the least square fitting, we obtain:

$$SIC\,PC1(t) = \beta_{AHT} AHT(t) + \beta_{AMT} AMT(t) + \beta_{OHT} OHT_{BSO}(t) \quad (8)$$

where β_{AHT} = 0.22, β_{AMT} = 0.21 and β_{OHT} = 0.22 are the standardized regression coefficients during 1960–2017 and t is time (year). The coefficient of multiple determination (R^2) is 0.31, and this model has passed F-test (statistically significant at the 99% level). The variance inflation factors (VIF) of the three variables are in turn 5.21, 4.79 and 1.45, which are smaller than 10, so there is not harmful collinearity between them[64]. By calculating the proportion of each standardized coefficient to the sum of three coefficients (Eq. 7), the relative contributions of atmospheric and oceanic transports to the interannual variability of SIC can be estimated as 66% and 34%, respectively.

Multiple linear regression model for the decadal variability of SIC

We also use a multiple linear regression model to estimate the relative contributions of 10-year low pass filtered BSO OHT, EG OHT and AO to the decadal variability of the Eurasian Arctic SIC in the form of

$$SIC\,PC2(t) = \beta_{AO} AO(t - \tau_{AO}) + \beta_{BSO} OHT_{BSO}(t - \tau_{BSO}) + \beta_{EG} OHT_{EG}(t) \quad (9)$$

where τ_{AO} or τ_{BSO} is the leading time when the AO or BSO OHT has a maximum correlation with the Eurasian Arctic SIC PC2. Here, τ_{AO} = 3 year and τ_{BSO} = 2 year are chosen. During 1960–2017, AO, BSO OHT and EG OHT have regression coefficients of −0.22, 0.43 and −0.50 with the Eurasian Arctic SIC PC2, whereas their corresponding VIFs are 1.48, 1.39 and 1.86. According to Eq. (7), it is estimated that the relative contribution of atmospheric (oceanic) transport to the decadal variability of the Eurasian Arctic SIC PC2 is 19% (81%) during 1960–2017. Similarly, we can also estimate the relative contributions of atmospheric and oceanic transports to the decadal variability of the Eurasian Arctic SIC PC2 during 1960–1999 and 2000–2017. It is found that the relative contributions of the atmospheric (oceanic) transport to the decadal Eurasian Arctic SIC PC2 during 1960–1999 and 2000–2017 are 12% and 48% (88% and 52%), respectively.

Data availability

The HadISST data are downloaded from https://www.metoffice.gov.uk/hadobs/hadisst/data/download.html. The ORAS5 data are available at https://www.cen.uni-hamburg.de/en/icdc/data/ocean/easy-init-ocean/ecmwf-oras5-backward-extension.html and https://www.cen.uni-hamburg.de/icdc/data/ocean/easy-init-ocean/ecmwf-oras5.html. The NCEP/NCAR data are available at https://psl.noaa.gov/data/gridded/data.ncep.reanalysis.html .

Code availability

The codes of the wavelet analysis are available at https://atoc.colorado.edu/research/wavelets/. And other source codes for the analysis of this study can be obtained upon request from the corresponding author.

Received: 20 November 2023; Accepted: 21 February 2024;
Published online: 06 March 2024

References

1. Comiso, J. C. Abrupt decline in the Arctic winter sea ice cover. *Geophys. Res. Lett.* **33**, L18504 (2006).
2. Comiso, J. C., Parkinson, C. L., Gersten, R. & Stock, L. Accelerated decline in the Arctic Sea ice cover. *Geophys. Res. Lett.* **35**, L01703 (2008).
3. Serreze, M. C., Holland, M. M. & Stroeve, J. Perspectives on the Arctic's shrinking sea-ice cover. *Science* **315**, 1533–1536 (2007).
4. Screen, J. A. & Simmonds, I. The central role of diminishing sea ice in recent Arctic temperature amplification. *Nature* **464**, 1334–1337 (2010).
5. Dai, A., Luo, D., Song, M. & Liu, J. Arctic amplification is caused by sea-ice loss under increasing CO_2. *Nat. Commun.* **10**, 121 (2019).
6. Francis, J. A. & Vavrus, S. J. Evidence linking Arctic amplification to extreme weather in mid-latitudes. *Geophys. Res. Lett.* **39**, L06801 (2012).
7. Walsh, J. E. Intensified warming of the Arctic: causes and impacts on middle latitudes. *Glob. Planet. Change* **117**, 52–63 (2014).
8. Cohen, J. et al. Recent Arctic amplification and extreme mid-latitude weather. *Nat. Geosci.* **7**, 627–637 (2014).
9. Mori, M., Watanabe, M., Shiogama, H., Inoue, J. & Kimoto, M. Robust Arctic sea-ice influence on the frequent Eurasian cold winters in past decades. *Nat. Geosci.* **7**, 869–873 (2014).
10. Vavrus, S. J. The influence of Arctic amplification on mid-latitude weather and climate. *Curr. Clim. Chang. Rep.* **4**, 238–249 (2018).

11. Overland, J. E. et al. Nonlinear response of mid-latitude weather to the changing Arctic. *Nat. Clim. Chang* **6**, 992–999 (2016).
12. He, S. P., Gao, Y. Q., Li, F., Wang, H. J. & He, Y. C. Impact of Arctic oscillation on the East Asian climate: A review. *Earth Sci. Rev.* **164**, 48–62 (2017).
13. Cavalieri, D. J. & Parkinson, C. L. Arctic sea ice variability and trends, 1979-2010. *Cryosphere* **6**, 881–889 (2012).
14. Parkinson, C. L., Cavalieri, D. J., Gloersen, P., Zwally, H. J. & Comiso, J. C. Arctic sea ice extents, areas, and trends, 1978–1996. *J. Geophys. Res. Oceans* **104**, 20837–20856 (1999).
15. Comiso, J. C. & Hall, D. K. Climate trends in the Arctic as observed from space. *Wiley Interdiscip. Rev. Clim. Change* **5**, 389–409 (2014).
16. Mahajan, S., Zhang, R. & Delworth, T. L. Impact of the Atlantic Meridional Overturning Circulation (AMOC) on Arctic Surface Air Temperature and Sea Ice Variability. *J. Clim.* **24**, 6573–6581 (2011).
17. Day, J. J., Hargreaves, J. C., Annan, J. D. & Abe-Ouchi, A. Sources of multi-decadal variability in Arctic sea ice extent. *Environ. Res. Lett.* **7**, 3 (2012).
18. Laxon, S., Peacock, N. & Smith, D. High interannual variability of sea ice thickness in the Arctic region. *Nature* **425**, 947–950 (2003).
19. Luo, B. et al. Origins of Barents-Kara sea-ice interannual variability modulated by the Atlantic pathway of El Niño–Southern Oscillation. *Nat. Commun.* **14**, 585 (2023).
20. Barton, B. I., Lique, C., Lenn, Y.-D. & Talandier, C. An Ice-Ocean model study of the mid-2000s regime change in the Barents Sea. *J. Geophys. Res. Oceans* **127**, e2021JC018280 (2022).
21. Notz, D. & Stroeve, J. Observed Arctic sea-ice loss directly follows anthropogenic CO_2 emission. *Science* **354**, 747–750 (2016).
22. Nakanowatari, T., Sato, K. & Inoue, J. Predictability of the barents sea ice in early winter: remote effects of oceanic and atmospheric thermal conditions from the North Atlantic. *J. Clim.* **27**, 8884–8901 (2014).
23. Onarheim, I. H., Eldevik, T., Årthun, M., Ingvaldsen, R. B. & Smedsrud, L. H. Skillful prediction of Barents Sea ice cover. *Geophys. Res. Lett.* **42**, 5364–5371 (2015).
24. Sigmond, M., Reader, M. C., Flato, G. M., Merryfield, W. J. & Tivy, A. Skillful seasonal forecasts of Arctic sea ice retreat and advance dates in a dynamical forecast system. *Geophys. Res. Lett.* **43**, 12457–12465 (2016).
25. Screen, J. A. & Francis, J. A. Contribution of sea-ice loss to Arctic amplification is regulated by Pacific Ocean decadal variability. *Nat. Clim. Change* **6**, 856–860 (2016).
26. Svendsen, L., Keenlyside, N., Bethke, I., Gao, Y. Q. & Omrani, N. E. Pacific contribution to the early twentieth-century warming in the Arctic. *Nat. Clim. Change* **8**, 793–797 (2018).
27. Kim, H., Yeh, S.-W., An, S.-I. & Song, S.-Y. Changes in the role of Pacific decadal oscillation on sea ice extent variability across the mid-1990s. *Sci. Rep.* **10**, 17564 (2020).
28. Jungclaus, J. H. & Koenigk, T. Low-frequency variability of the arctic climate: the role of oceanic and atmospheric heat transport variations. *Clim. Dyn.* **34**, 265–279 (2010).
29. Beitsch, A., Jungclaus, J. H. & Zanchettin, D. Patterns of decadal-scale Arctic warming events in simulated climate. *Clim. Dyn.* **43**, 1773–1789 (2014).
30. Årthun, M., Eldevik, T., Smedsrud, L. H., Skagseth, O. & Ingvaldsen, R. B. Quantifying the influence of Atlantic Heat on Barents Sea Ice Variability and Retreat. *J. Clim.* **25**, 4736–4743 (2012).
31. van der Linden, E. C., Bintanja, R., Hazeleger, W. & Graversen, R. G. Low-frequency variability of surface air temperature over the Barents Sea: causes and mechanisms. *Clim. Dyn.* **47**, 1247–1262 (2016).
32. Olonscheck, D., Mauritsen, T. & Notz, D. Arctic sea-ice variability is primarily driven by atmospheric temperature fluctuations. *Nat. Geosci.* **12**, 430–434 (2019).
33. Deser, C., Walsh, J. E. & Timlin, M. S. Arctic sea ice variability in the context of recent atmospheric circulation trends. *J. Clim.* **13**, 617–633 (2000).
34. Strong, C., Magnusdottir, G. & Stern, H. Observed feedback between Winter Sea Ice and the North Atlantic Oscillation. *J. Clim.* **22**, 6021–6032 (2009).
35. Gong, T. & Luo, D. Ural blocking as an amplifier of the Arctic Sea Ice decline in Winter. *J. Clim.* **30**, 2639–2654 (2017).
36. Luo, B., Luo, D., Wu, L., Zhong, L. & Simmonds, I. Atmospheric circulation patterns which promote winter Arctic sea ice decline. *Environ. Res. Lett.* **12**, 054017 (2017).
37. Lien, V. S., Schlichtholz, P., Skagseth, O. & Vikebo, F. B. Wind-driven Atlantic water flow as a direct mode for reduced Barents Sea Ice cover. *J. Clim.* **30**, 803–812 (2017).
38. Beszczynska-Moeller, A., Woodgate, R. A., Lee, C., Melling, H. & Karcher, M. A synthesis of exchanges through the main oceanic gateways to the Arctic Ocean. *Oceanography* **24**, 82–99 (2011).
39. Rudels, B. et al. Circulation and transformation of Atlantic water in the Eurasian Basin and the contribution of the Fram Strait inflow branch to the Arctic Ocean heat budget. *Prog. Oceanogr.* **132**, 128–152 (2015).
40. Smedsrud, L. H., Sirevaag, A., Kloster, K., Sorteberg, A. & Sandven, S. Recent wind driven high sea ice area export in the Fram Strait contributes to Arctic sea ice decline. *TC* **5**, 821–829 (2011).
41. Chen, X., Luo, D., Feldstein, S. B. & Lee, S. Impact of winter ural blocking on Arctic Sea Ice: short-time variability. *J. Clim.* **31**, 2267–2282 (2018).
42. Deser, C., Alexander, M. A., Xie, S. P. & Phillips, A. S. Sea surface temperature variability: patterns and mechanisms. *Annu Rev. Mar. Sci.* **2**, 115–143 (2010).
43. Kushnir, Y. et al. Atmospheric GCM response to extratropical SST anomalies: synthesis and evaluation. *J. Clim.* **15**, 2233–2256 (2002).
44. Polyakov, I. V. et al. Greater role for Atlantic inflows on sea-ice loss in the Eurasian Basin of the Arctic Ocean. *Science* **356**, 285–191 (2017).
45. Zhang, R. et al. A review of the role of the atlantic meridional overturning circulation in atlantic multidecadal variability and associated climate impacts. *Rev. Geophys.* **57**, 316–375 (2019).
46. Polyakov, I. V. et al. Arctic ocean warming contributes to reduced polar ice cap. *J. Phys. Oceanogr.* **40**, 2743–2756 (2010).
47. You, C., Tjernstrom, M., Devasthale, A. & Steinfeld, D. The role of atmospheric blocking in regulating Arctic Warming. *Geophys. Res. Lett.* **49**, 12 (2022).
48. Cai, Q., Beletsky, D., Wang, J. & Lei, R. Interannual and decadal variability of arctic summer sea ice associated with atmospheric teleconnection patterns during 1850–2017. *J. Clim.* **34**, 9931–9955 (2021).
49. Li, Y. et al. Observed contribution of Barents-Kara sea ice loss to warm Arctic-cold Eurasia anomalies by submonthly processes in winter. *Environ. Res. Lett.* **18**, 034019 (2023).
50. Zhao, J. & Johns, W. Wind-forced interannual variability of the Atlantic meridional overturning circulation at 26.5°N. *J. Geophys. Res. Oceans* **119**, 2403–2419 (2014).
51. Årthun, M., Asbjornsen, H., Chafik, L., Johnson, H. L. & Våge, K. Future strengthening of the Nordic Seas overturning circulation. *Nat. Commun.* **14**, 2065 (2023).
52. Luo, D. H. et al. Weakened potential vorticity barrier linked to recent Winter Arctic Sea Ice loss and midlatitude cold extremes. *J. Clim.* **32**, 4235–4261 (2019).
53. Xu, X. P., He, S. P., Zhou, B. T., Wang, H. J. & Sun, B. Arctic warming and Eurasian cooling: weakening and reemergence. *Geophys. Res. Lett.* **50**, e2023GL105180 (2023).
54. Heukamp, F. O. et al. Cyclones modulate the control of the North Atlantic Oscillation on transports into the Barents Sea. *Commun. Earth Environ.* **4**, 324 (2023).
55. Rayner, N. A. et al. Global analyses of sea surface temperature, sea ice, and night marine air temperature since the late nineteenth century. *J. Geophys. Res. Atmos.* **108**, 4407 (2003).
56. Zuo, H., Balmaseda, M. A., Tietsche, S., Mogensen, K. & Mayer, M. The ecmwf operational ensemble reanalysis-analysis system for

ocean and sea ice: a description of the system and assessment. *Ocean Sci.* **15**, 779–808 (2019).
57. Kalnay, E. et al. The NCEP/NCAR 40-year Reanalysis project. *Bull. Am. Met. Soc.* **77**, 437–472 (1996).
58. Roberts, J. & Roberts, T. D. Use of Butterworth low-pass filter for oceanographic data. *J. Geophys. Res. Oceans* **83**, 5510–5514 (1978).
59. Torrence, C. & Compo, G. P. A practical guide to wavelet analysis. *Bull. Am. Meteorol. Soc.* **79**, 61–78 (1998).
60. Oldenburg, D., Armour, K. C., Thompson, L. & Bitz, C. M. Distinct mechanisms of ocean heat transport Into the Arctic Under internal variability and climate change. *Geophys. Res. Lett.* **45**, 7692–7700 (2018).
61. Metz, W. Optimal relationship of large-scale flow patterns and the barotropic feedback due to high-frequency eddies. *J. Atmos. Sci.* **48**, 1141–1159 (1991).
62. Darlington, R. B. Regression and Linear Models; McGraw-Hill: New York, NY, USA, (1990).
63. Newman, T. & Browner, W. J. E. In defense of standardized regression coefficients. *Epidemiology* **2**, 383–386 (1991).
64. Mason, C. H. & Perreault, W. D. Collinearity, power, and interpretation of multiple regression analysis. *J. Mark. Res.* **28**, 268–280 (1991).

Acknowledgements

This research was supported by the National Natural Science Foundation of China (Grant numbers: 42288101; 42150204 and 41875073). B. Luo was supported by the China National Postdoctoral Program for Innovative Talents (BX20230045) and the China Postdoctoral Science Foundation (2023M730279).

Author contributions

J. Shi performed this study, plotted all figures and wrote the preliminary manuscript in part, D. Luo supervised this manuscript and revised the preliminary manuscript. B. Luo, Y. Yao, T. Gong and Y. Liu joined this study and gave some discussions on the improvement of this manuscript. All the authors contributed to the writing and reviewing of the manuscript.

Competing interests

The authors declare no competing interests.

Additional information

Supplementary information The online version contains Supplementary Material available at https://doi.org/10.1038/s41612-024-00605-5.

Correspondence and requests for materials should be addressed to Dehai Luo.